Hindawi
Advances in Civil Engineering
Volume 2020, Article ID 6102062, 11 pages
https://doi.org/10.1155/2020/6102062

Research Article

The Real-Time Automated Monitoring System for Lateral Deflection of Underground Structures

Hang Chen,[1] Huqing Liang,[2] Mengxiong Tang,[1] Sheng Jiang,[3] and Hesong Hu[1]

[1]*Guangzhou Institute of Building Science Co., Ltd., Guangzhou 510440, China*
[2]*Guangzhou Municipal Construction Group Co., Ltd., Guangzhou 510440, China*
[3]*College of Electronic Engineering, South China Agricultural University, Guangzhou 510642, China*

Correspondence should be addressed to Hesong Hu; hhs@gibs.com.cn

Received 19 September 2019; Revised 14 February 2020; Accepted 17 February 2020; Published 23 March 2020

Academic Editor: Venu G. M. Annamdas

The lateral wall deflection is the most intuitive parameter to reveal the stability and safety of underground excavations. The existing automated approaches, such as to serialize dozens of inclinometers along casing pipes, are too expensive to be applied in most common projects. To guarantee stable automation and lower the costs, a novel system based on strain measurement is proposed in this paper to achieve real-time automated monitoring of underground excavations. The specially designed components are highlighted to benefit the mass industrial production and rapid *in situ* assembly. By theoretical comparisons, the accuracy and resolution performance of the proposed strategy are demonstrated to be better than those of the traditional manual method. The applicability of the mentioned system was verified by an engineering case, from which it was demonstrated that the proposed system works well to predict the lateral wall deflection of underground excavations. The sensitivity of the monitored results to the boundary conditions is also carefully discussed. The designed system has broad application prospects to provide timely data for safety assessment to prevent the unexpected failure of underground excavation as well as other engineering structures with dangerous lateral deflection or movement.

1. Introduction

The complexity of ultradeep structures in urban areas with dense existing buildings raises very serious safety risks during the construction stage. The accidents of excavation or slope collapse were reported every year in different provinces of China as well as other countries and areas with large population or complex geological conditions [1–6]. From 2015 to 2017 in China, 11.3% of the total accidents in construction projects are accounted for excavation collapse, where 68 people were killed [7–9]. According to the lessons learnt from a large amount of cases, almost all of the accidents were symptomatic before their occurrence [1, 10, 11]. However, according to the Chinese national standard *Technical Code for Monitoring of Foundation Pit Engineering* [12], the maximum monitoring frequency under normal conditions is just 2~3 times per day due to the limitation of existing monitoring techniques, which have fallen behind the industrialization level, especially in developing countries, so that real-time data analysis and visualization have not been implemented to date [13, 14]. Therefore, to be the last guard to ensure construction safety, the monitoring techniques have attracted unprecedented attentions from scientists and engineers to develop theories, models, methods, and equipment to provide both sufficiently timely alarms before the accidents and scientific accident analysis [15–27].

The lateral wall deflection is the most intuitive parameter to reveal the stability and safety of underground excavations. To realize real-time data collection, the existing solutions are to install several cores of the precise inclinometers [22–24] and distribute fibre Bragg gratings (FBG) [25–27] along the casing pipes, both of which are too expensive to be applied in common commercial or residential projects. The automated positioning technologies with high precision, such as radio frequency identification (RFID), interferometric synthetic aperture radar (InSAR), and real-time kinematic global

positioning system (RTK-GPS), are also continuously attempted [28–30], but neither of them can satisfy the precision requirement (i.e., submillimetre) enforced by specifications. Therefore, it is of great importance to develop a set of cost-effective and reliable real-time automated systems to monitor the lateral deflection of the excavations in order to provide timely warnings in case of dangers.

In this paper, an automated system based on strain gauges and specially designed measuring pipes is designed, which greatly reduced the monitoring costs when compared to existing automated strategies. The accuracy and resolution of the proposed strategy is analyzed, and its applicability of the mentioned system was verified by an engineering case. The sensitivity of the monitored results to the boundary conditions is also carefully discussed.

2. Materials and Methods

2.1. Design of the System. The traditional inclinometers are based on the angle measurement, where the inclination sensing unit is packaged into a metal shell. The manual measurement is to record the inclination at different depths (with a constant spacing l) of the casing pipes, which is defined as θ_i at the ith measuring point starting at the pipe's toe. The linear integral gives the deflection of the casing pipes as

$$w_i(L - kl) = \sum_{i=1}^{k} l \sin \theta_i, \tag{1}$$

where $L - kl$ is the depth coordinate with the origin at the pipe head. As the manual method is highly commercialized, in general, the supporting software can directly give the deflection. It is suggested by the Chinese national standard [12] that the accuracy and resolution are not lower than 0.25 mm/m and 0.02 mm/500 mm, which indicates that the accuracy and resolution of the inclination sensor are larger than 0.014 and 0.002 degree. In addition, the inclinometers should have a very reliable waterproof ability because the casing pipes are not well sealed. Therefore, the accuracy requirement and complex waterproof design lead to the expensive cost of inclinometers. Moreover, if the deflection of the casing pipes is larger or the cross sections of the pipes experience excessive deformation induced by surrounding strata or concrete, the inclinometers cannot be inserted into the desired depth of the casing pipes. If additional power is employed to deliberately complete the insertion, the inclinometers may be stuck in the pipes during the next measurement backhaul.

Compared to angle measurement, the strain gauges are cheap enough to be applied in a large scale of engineering projects. However, the strain measurement is one of the typical contact measurement methods. Both of the inner and outer surfaces of traditional casing pipes are faced to harsh environment so that the strain gauges are impossible to survive on the pipes. On the other hand, as both the power supply and voltage measurement are involved in strain measurement, complicated physical wires corresponding to the strain gauges are easy to be damaged up to dozens of meters during splicing installation. Therefore, it is necessary to come up with special designs to solve the problems mentioned above.

Both the strain gauges and corresponding electrical components need a dry environment to avoid damage by underground water. Therefore, double-layer measuring pipes are designed in this paper to create a sealing space in inner pipes, as shown in Figure 1. Traditional commercial casing pipes are employed as the outer protective layer to prevent the inner pipes from being damaged by underground risk factors. To reveal the real deformation of the measured structures or strata, the deflection of the inner pipes should be compatible with that of the outer casing pipes. Therefore, the profile of the inner pipes made of polyvinyl chloride (PVC) by the cold-extrusion method (as shown in Figure 2(a)) exactly matches the troughs of generic commercial casing pipes. For the convenience of industrial production, the inner pipes are fabricated to the same specific length as that of the commercial casing pipes, e.g., 1 m, 2 m, and 4 m. The injection-molded waterproof connectors are designed for inserted installation to connect the inner pipes, as shown in Figure 2(b). Embedded tapping screws are employed to fix the connectors and inner pipes, and the rubber loops can prevent water from entering the core of inner pipes through the screw holes on the outer casing pipes. For consistency with the system assembly, the inner circle of the inner pipes at their ends is processed to be a standard circle with the radius same as the outer radius of the connectors. In summary, the design of the double-layered measuring pipes, including commercial casing pipes, inner pipes, and waterproof connectors, can provide ideal environments for the sensors (i.e., strain gauges) and related circuits.

On the other hand, it is difficult to paste the strain gauges on the inner surface of the inner pipes. If the inner pipes are designed as spliced semicylindrical, the efforts and costs of the corresponding waterproof measures will drastically increase. Therefore, strain strips, made of the printed circuit board (PCB) as shown in Figure 2(c), with pasted strain gauges are prefabricated and assembled into the four parallel partially open troughs, which are evenly distributed around the inner surface of the inner pipes. In general, the spacing of the strain gauges is 0.5 m, which is consistent with traditional manual measurement. Besides, printed circuits with ~10 μm thickness and ~100 μm width are arranged on the PCB with pasted gauges to replace the traditional wires to connect the strain gauges and measurement circuits along the entire measuring pipes so that the core of the inner pipes is no longer crowded and in chaos. The measuring circuits (Wheatstone bridges) of all the strain gauges in a single pipe are also integrated on PCBs (Figure 2(d)), which are fabricated and contained in the waterproof connectors by using hollow plates. At each cross section to be measured, two pairs of face-to-face strain gauges, which are connected to the neighbouring arms of the same Wheatstone bridge in order to calculate the difference, are arranged so that each PCB of measuring circuits has eight Wheatstone bridges for 2 m-size measuring pipes (i.e., two bending directions and four different cross sections to be measured). A cable, that

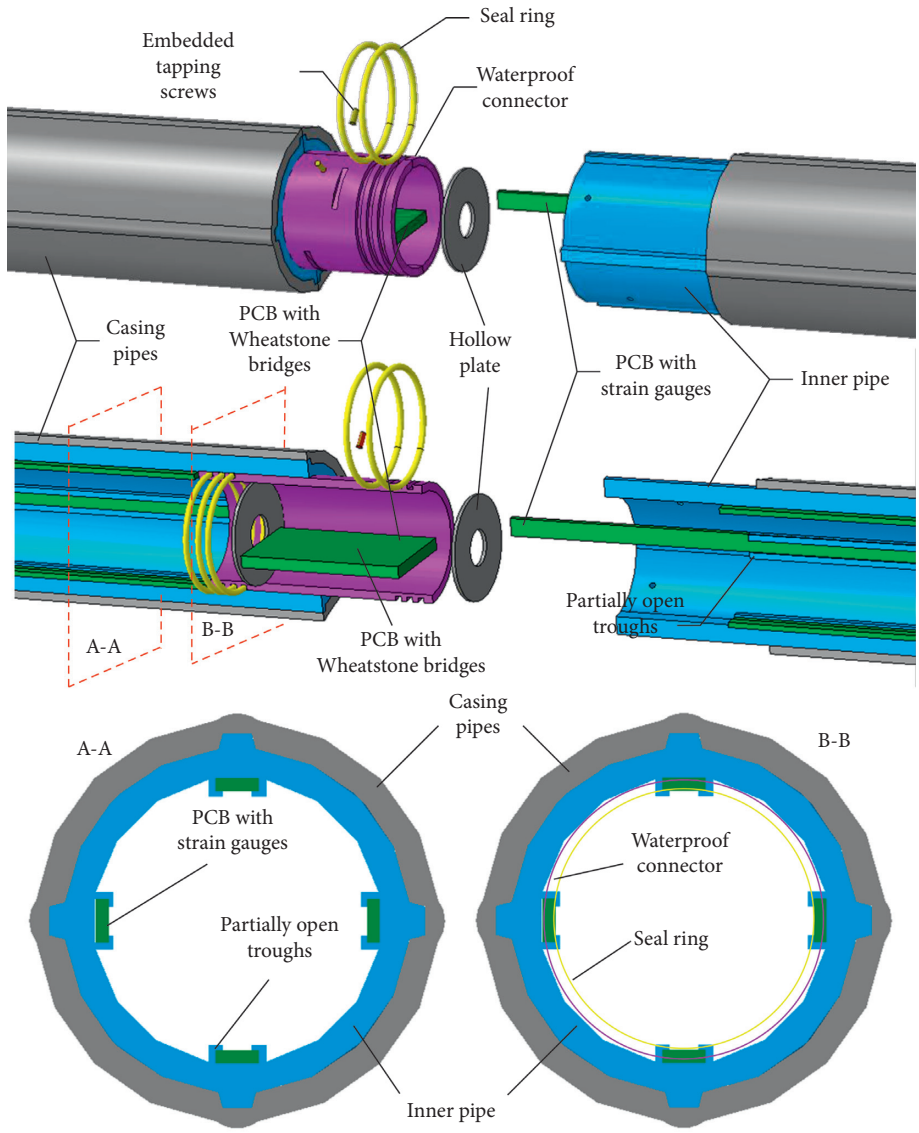

Figure 1: Schematic diagram of the structure of the double layered measuring pipes.

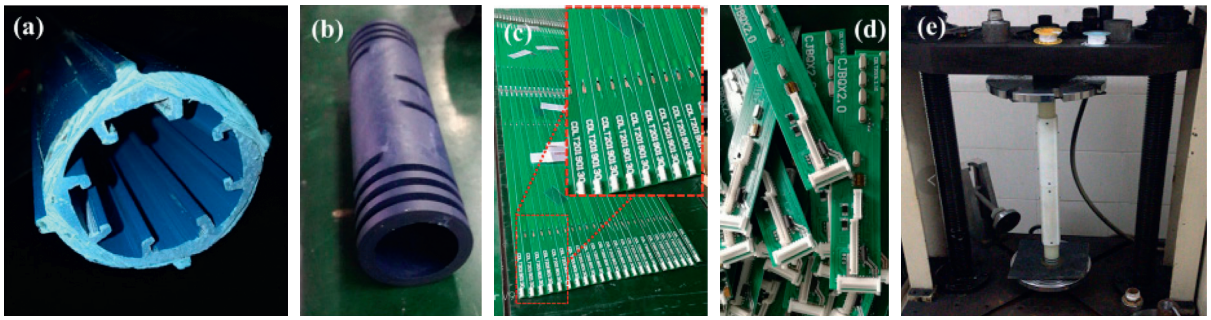

Figure 2: Photographs of (a) the cross section of the inner pipes, (b) PCBs with strain gauges, (c) PCBs with Wheatstone bridges, (d) waterproof connector, and (e) waterproof test.

provides power for the strain measurement and path for the data transmission, serializes the PCBs with Wheatstone bridges in each waterproof connector.

On the top of the double-layered pipes (above the ground), only one inclinometer is installed to provide boundary condition for subsequent data processing, which is

discussed in detail in the next section. Both the digital responses of the Wheatstone bridges and the inclinometer are collected by using a data integrator and send to a gateway through local area network. Figure 3 shows the structure of the electronic components of the proposed automated system at a certain measuring point. The gateway, connected with multiple data integrators as shown in Figure 4, can store the monitored data as a backup, be sent to platform by general packet radio service (GPRS), and transmit the orders from the command centre of the platform to data integrators.

2.2. Mechanism of the System. The coordinate system employed in subsequent theoretical analysis is schematically shown in Figure 5. For any given depth $z = h_i$ ($i = 1, 2, \ldots, n$, where n is the total number of the measured cross section), the monitored strains corresponding to the positive and negative directions of the x and y axes of the system are, respectively, defined as ε_{ix+}, ε_{ix-}, ε_{iy+}, and ε_{iy-}, as shown in Figure 5(b). The bending strain, defined as the output of the Wheatstone semibridge where the two mutative resistances are located on adjacent bridge arms, presents as

$$\begin{cases} \varepsilon_{ix}^{b} = -\varepsilon_{ix+} + \varepsilon_{ix-}, \\ \varepsilon_{iy}^{b} = -\varepsilon_{iy+} + \varepsilon_{iy-}. \end{cases} \tag{2}$$

Then, one can get the curvature of the pipes at the measured section as

$$\begin{cases} \kappa_{ix}^{b} = \dfrac{\varepsilon_{ix}^{b}}{D_0}, \\ \kappa_{iy}^{b} = \dfrac{\varepsilon_{iy}^{b}}{D_0}, \end{cases} \tag{3}$$

where D_0 is the radius of the circumference the strain gauges are located in (i.e., the radius of the red circle in Figure 5(b)). In this linear problem of a slender beam with large deflection and small deformation, the derivation from the curvature to the deflection in x and y directions is independent from each other. Therefore, only the details related to x direction is discussed and the subscript "x" is omitted in the subsequent part.

According to the differential equation of an in-plane bending slender beam under small deformation, the rotation angle θ and curvature κ are the first- and second-order derivatives of the deflection w, respectively, i.e.,

$$\kappa_i(z) \approx \frac{\mathrm{d}[\theta_i(z)]}{\mathrm{d}z} \approx \frac{\mathrm{d}^2[w_i(z)]}{\mathrm{d}z^2}. \tag{4}$$

Trapezoidal rule is employed to establish the numerical integration to obtain the rotation angle as

$$\theta_i = \theta_i(z = h_i) = \sum_{k=1}^{i-1} \frac{1}{2}\kappa_k (h_{k+1} - h_{k-1}) + \frac{1}{2}\kappa_i (h_i - h_{i-1}) + \theta_0, \tag{5}$$

where $\kappa_0 = 0$ due to the free pipes' head, θ_0 is the rotation angle measured by using the inclinometer installed at pipes' head, and $h_0 = 0$. Generally, the depth of the inclination pipes should be large enough to be socketed in the rocks so that the absolute displacement of the pipes toe is approximated to be zero. If the socketed condition is not allowed in some unpredictable situations, one can also measure the displacement at the pipes' head instead. Subsequently, for the two different boundary conditions mentioned above, the numerical integration from curvature to deflection presents as

$$w_i = w(z = h_i) = \frac{1}{2}\theta_0 (h_1 - h_0) + \sum_{k=1}^{i-1} \frac{1}{2}\theta_k (h_{k+1} - h_{k-1}) + \frac{1}{2}\theta_i (h_i - h_{i-1}) + C, \tag{6}$$

where (1) if the displacement at the pipes' head is measured

$$C = w_0 = w(h_0 = 0); \tag{7}$$

and (2) for the socketed cases,

$$C = -\left[\frac{1}{2}\theta_0 (h_1 - h_0) + \sum_{k=1}^{n-1} \frac{1}{2}\theta_k (h_{k+1} - h_{k-1}) + \frac{1}{2}\theta_n (h_n - h_{n-1})\right]. \tag{8}$$

The resolution of the strain gauges is $r = 1\mu\varepsilon$, which gives the resolution of the measuring pipe (with the spacing of the measured cross section as $L_0 = 500$ mm) as $rL_0^2/D_0 \approx 0.004$ mm (where $D_0 \approx 60$ mm). Assuming that the error of the bending strain is δ, the displacement error of the single measuring pipe should be $\delta L_0^2/D_0$. If the accuracy of the mentioned system is not larger than that required by the traditional manual method (i.e., 0.125 mm/500 mm), one can get $\delta < \delta_0 = 30\,\mu\varepsilon$. In other words, as the error of the commonly used strain gauges is about 1%~2% of the displayed value, the accuracy of the traditional manual method is better than that of the mentioned automated system as long as the bending strain Δ exceeds $1500\sim3000\mu\varepsilon$. However, under such circumstance (i.e., $\Delta > 1500\sim3000\,\mu\varepsilon$), the deflection of a single measuring pipe ($L_0 = 500$ mm) reaches $\Delta L_0^2/D_0 = 6.25 \sim 12.5$ mm, which is too exaggerated for its application to underground excavation or slope engineering. Therefore, from the aspect of engineering practice, both of the accuracy and resolution of the proposed strain-based measurement system is larger than that of the traditional manual method.

2.3. Procedures of Deflection Measurement. Figure 6 shows the steps from the instrument installation to complete the measurement. One of the special designs is the assignment of unique ID for each measured cross section and direction. During the *in situ* assembly process, the orders and directions of the inner pipes are automatically recorded and input into the platform by supporting software so that the deflection can be correctly calculated. The commercial casing pipes and inner pipes are also synchronously installed to keep the same total length. Moreover, as the bending strains are defined as the difference between the coupled strain gauges measured by Wheatstone semibridges, temperature-induced zero drift can be mechanistically eliminated.

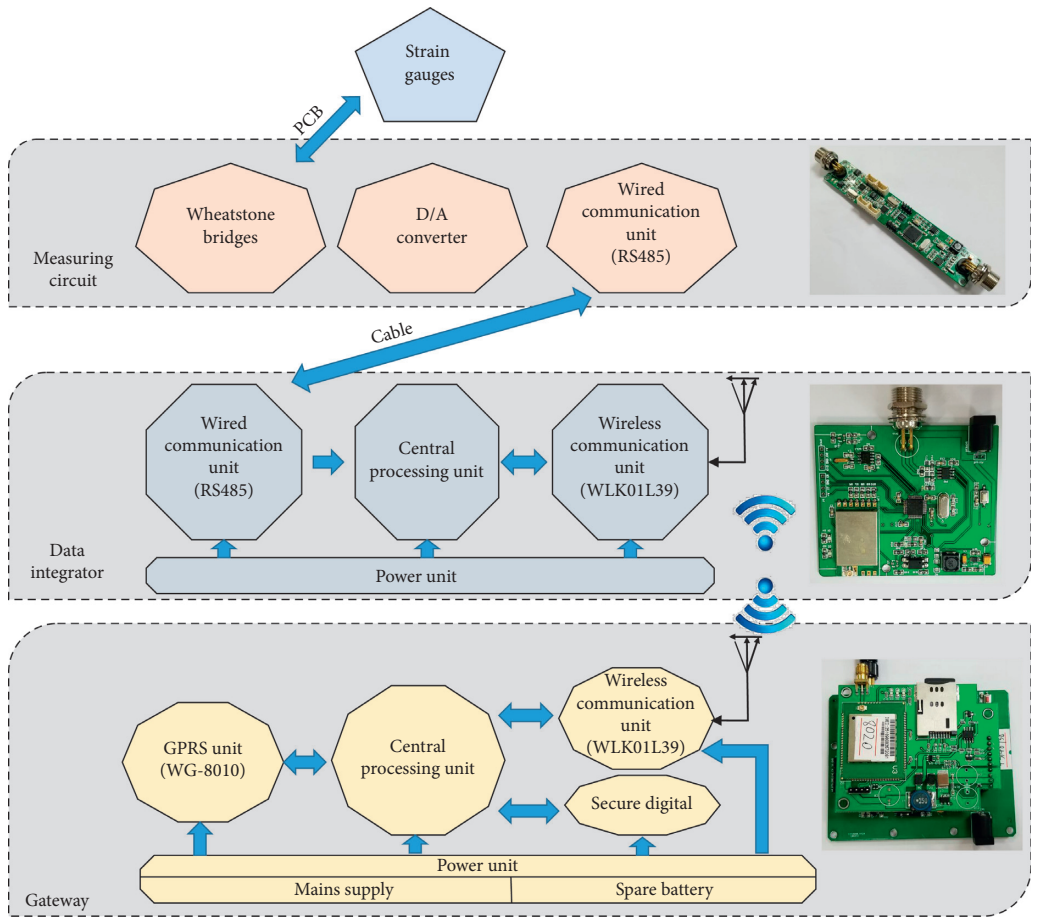

FIGURE 3: Structures and photographs of the electronic components of the proposed automated system.

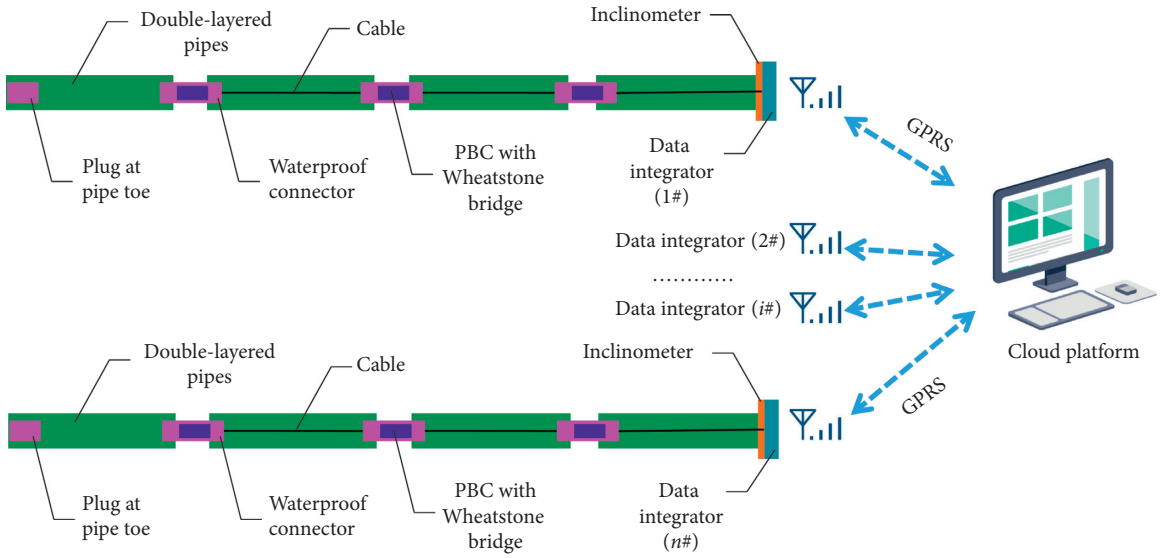

FIGURE 4: Schematic diagram of the assembly of special designed pipes and electronic components.

3. Results and Discussion

The applicability of the mentioned system was verified by an engineering case, where the results given by traditional measurement and the proposed automated system in this paper were compared. The engineering case is a twenty-story tower hotel with the underground structure of three stories and one mezzanine. The perimeter, depth, and area of the

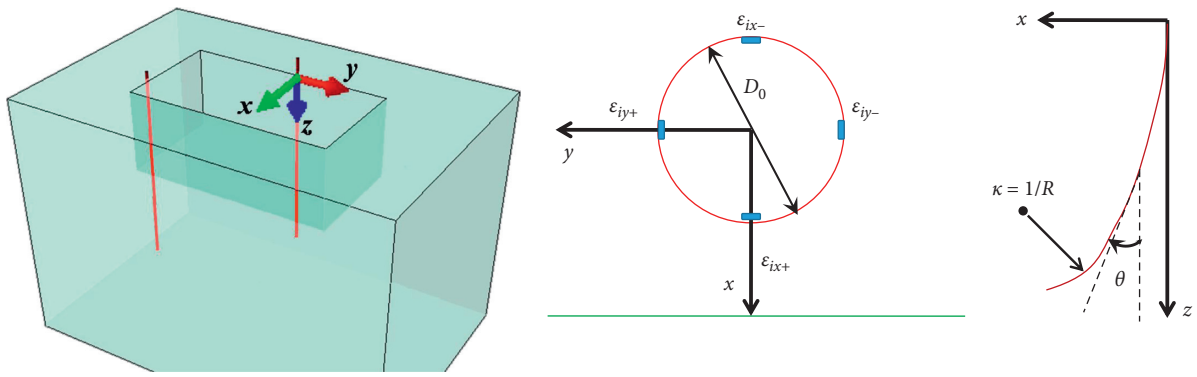

Figure 5: Coordinate system in the theoretical analysis.

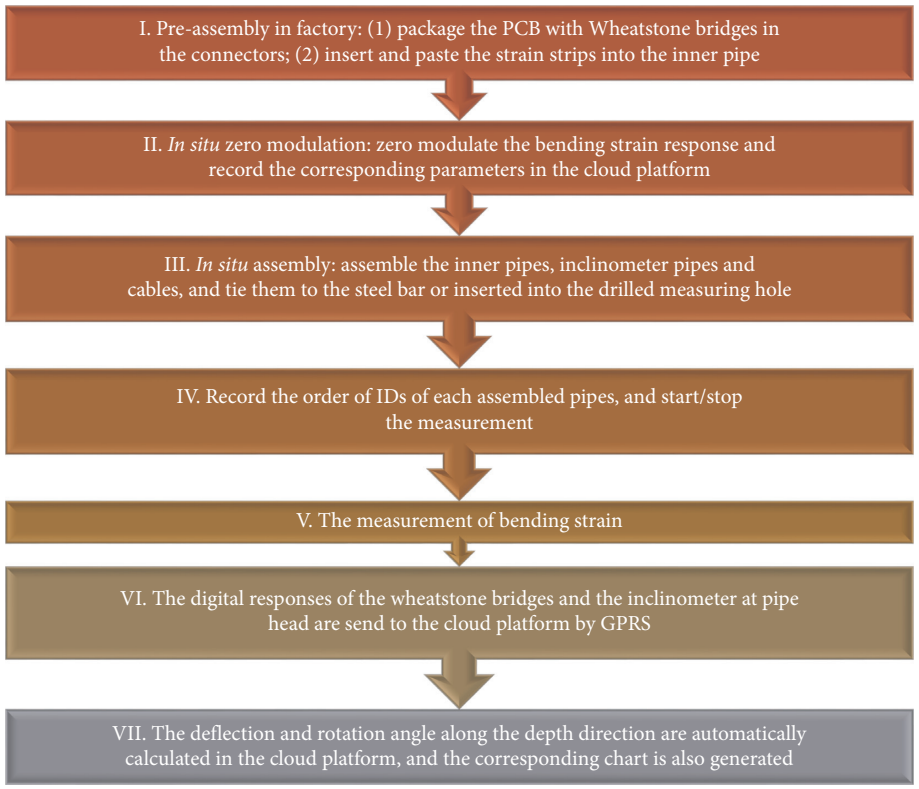

Figure 6: Flow chart of the measurement.

designed rectangular foundation excavation is about 331 m, 17.9 m~18.4 m, and 7747.35 m^2, respectively, as shown in Figure 7. The combination of cast-in-situ piles, steel angle braces in corners, and local anchors is the basic form of the support structures. The monitoring stage began in July 2017 and ended in December 2018 (when backfilling works have been done), as listed in Table 1. Seventeen measured points (J1~J17 in Figure 7) are almost evenly distributed along the perimeter of the foundation excavation, where four of them are chosen to be investigated in detail (as highlighted by red in Figure 7, i.e., J2, J9, J12, and J16). Each pair of the proposed automated system and the traditional casing pipes for comparison purpose are embedded in a certain retaining pile with the spacing of 300 mm (~4 times the pipe diameter). The comparisons cover both the midpoints and corners and include samples of four excavation sides.

The measuring points J2 and J16 near the midpoints of excavation sides (more dangerous related to construction security), where both of the automated measuring pipes and traditional casing pipes for comparison purpose reach 20.0~22.0 m, were bonded to reinforcement of the retaining piles and then embedded in concrete before the excavation construction. According to local experiences and economic reasons, the measured points J9 and J12 with only about 14.0 m depth were completed during the excavation construction (between S2 and S3, i.e., embedded into drilled

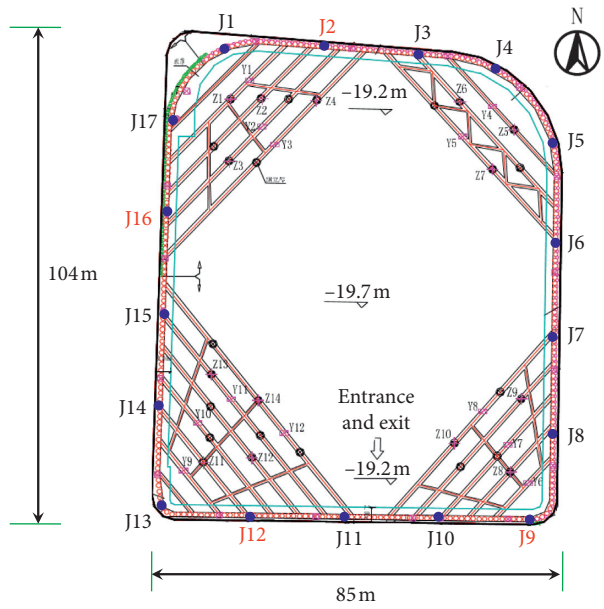

Figure 7: Dimensions and measured point distribution in the studied case.

Table 1: The progress summaries in typical construction stages.

Date	Construction progress summaries
2017-07-11 (S0)	Monitoring system installation and zero modulation of J2 and J16 are completed.
2017-09-11 (S1)	The depth of the middle and northern parts of the excavation is about 4 m and 5 m, respectively. Supporting structures in south part of the west side are being constructed.
2017-11-11 (S2)	The depth of the west and north parts of the excavations is about 13 m. Monitoring system installation and zero modulation of J9 and J12 are completed.
2018-01-11 (S3)	The depth of the whole excavation is about 13 m. The second layer of the support structure in the southwest corner is under construction.
2018-03-10 (S4)	The local depth of some parts of the excavation reaches the designed depth.
2018-07-11 (S5)	The depth of the whole excavation reaches the designed value. Raft structures are being constructed in some local parts.
2018-09-12 (S6)	Underground structures are being constructed. Support structures in the southwest corner have been removed.
2018-12-25 (S7)	The core structure above ground is being constructed. The excavation except for some eastern local parts has been backfilled.

holes in retaining piles) and discarded after the second layer of support structures were removed (i.e., stage S6). It should be noted that all the parameters to character the deformation of the pipes are based on the zero modulation after completing the instrument installation. All the data in the following analysis are collected at about 11 : 00 am.

The curvatures along the measuring pipes calculated by the directly measured bending strains divided by the D_0 are shown in Figure 8. Figures 9 and 10 show the comparison of rotation angle and deflection results between the proposed automated system and the traditional manual method during several typical construction stages (i.e., S0~S6 in Table 1). Although larger fluctuations of the rotation angle given by the automated system are presented, which directly related to the fluctuations of the recorded bending strain, the overall trend of the rotation angle by the automated system along the depth direction is well consistent with that given by the traditional manual method. Moreover, the fluctuations became severer as construction continues. Through endurance tests, where a single measuring pipe was bending to a given curvature (i.e., 0.005 m^{-1}), the intimate cooperation between the strain strips and corresponding open troughs on the inner surface of the inner pipes gradually appeared due to the aging of adhesive and mismatch thermal expansion so that the fluctuations were observed. Therefore, more technical measures should be taken to guarantee the deformation compatibility between the strain strips and inner pipes. The integrated deflections given by the automated system in the subfigures in first and second lines of Figure 10 are, respectively, based on measured pipes' head displacement (i.e., Equations (6) and (7)) and socketed condition (i.e., Equations (6) and (8)). It is found that the

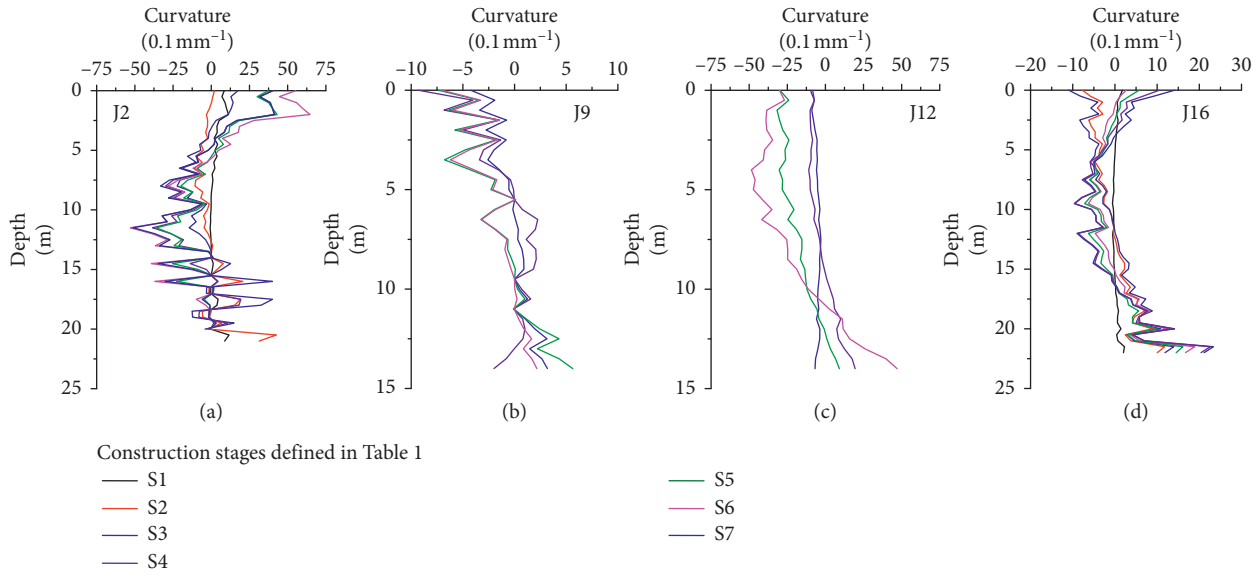

Figure 8: Directly measured bending strains at several typical construction stages in the studied case.

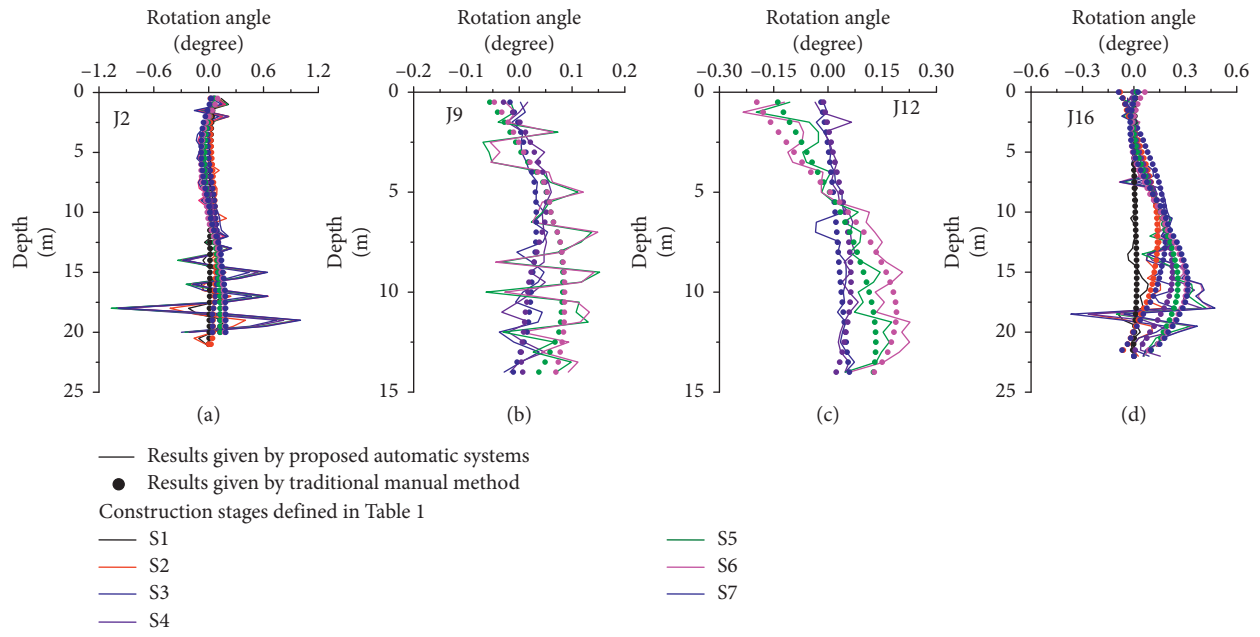

Figure 9: Comparison of the rotation angle between the proposed automated system and traditional manual method at several typical construction stages in the studied case.

variation tendency of the lateral deflection perpendicular to the excavation sides predicted by the mentioned automated system is always consistent with that of the traditional method. It is also indicated that the results are sensitive to boundary conditions. The automatically measured deflection base on the socketed condition (Figures 10(a)~10(d)) generally matches better with that measured by the traditional manual method, because the algorithm in the traditional manual method is also based on socketed condition. It should be pointed out that the measured pipes' head displacement is almost relative to the geodetic coordinate system, because the measurement is based on the national plane control network. From this point, the displacement referenced is called "absolute" displacement in subsequent sections.

For the first installed measuring points J2 and J16, except when the overall deflection along the pipes is relatively small (e.g., S2 shown by red lines), the measured displacement at pipes' head is almost consistent with that predicted by socketed condition, as shown in Figures 10(e) and 10(h). This is because the total length of measuring pipes (i.e., the double-layered pipes in the mentioned automated system

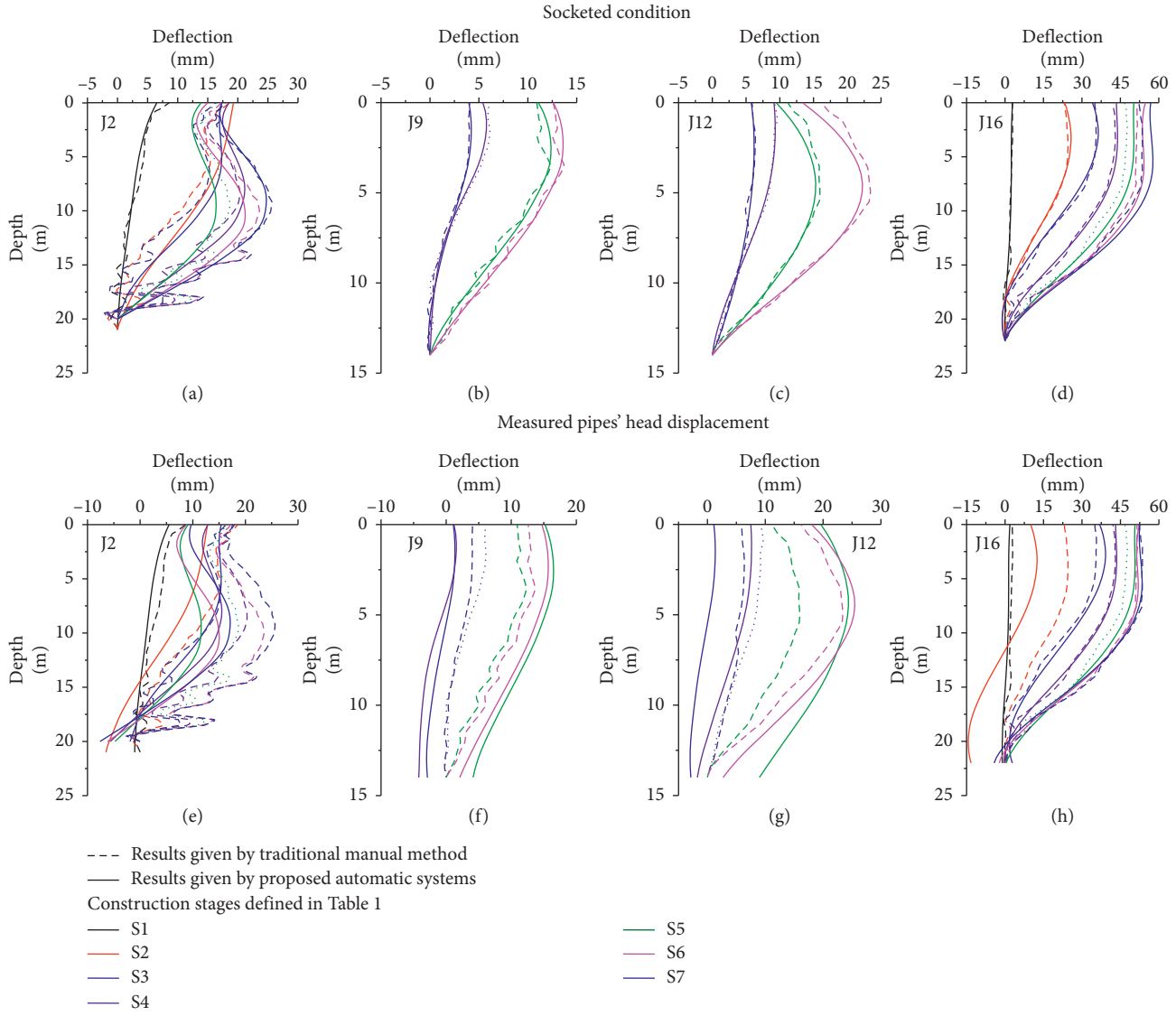

Figure 10: Comparison of the monitored results between the proposed automated system and traditional manual method at several typical construction stages in the studied case.

and separate commercial casing pipes for the traditional manual method) is long enough to activate the socketed condition.

However, in the initial stage of construction (e.g., S2 shown by red lines), the depth related to absolute zero lateral displacement (about 15 m for J2 and 12 m for J16) is approximately equal to the excavation depth (~13 m) at that time. Below the working plane of the excavation, the pipes as well as the retaining piles deform outward the excavation. In other words, the socketed condition at the pipes' toe is no longer established and the absolute displacement at pipes' toe is negative (i.e., move outward the centre of the excavation). The same phenomenon is also found in the stages S3 and S4 of measuring points J9 and J12 (shown by blue and purple lines in Figures 10(f) and 10(g)). Moreover, the value of the negative absolute displacement at the pipes' toe in S2 of J2 and J16 (red solid lines in the first and fourth rows of Figure 10) is larger than that in S3 and S4 of J9 and J12 (shown by blue and purple lines in Figures 10(e) and 10(h)). This is because the former cases have deeper pipe toes and experience more corresponding excavation progresses from the completion of instrument installation to the measuring date (i.e., about 13 m from S0 to S2 of J2 and J16 and <7 m from S3 to S4 of J9 and J12).

As all the sections of measuring points J9 and J12 (0~16 m in depth) are above the final working plane (~19 m in depth), the point corresponding to zero absolute displacement is gradually lower than the pipes' toe in subsequent stages S5 and S6, i.e., positive absolute displacement at the pipes' toes. Therefore, the overall displacement based on pipes' head displacement is larger than that with socketed condition, as shown by Figures 10(f) and 10(g).

In summary, both the two different boundary conditions work well to predict the vertical profile of the deflection, which is also consistent with the traditional manual method. However, it is indicated that the results are sensitive to

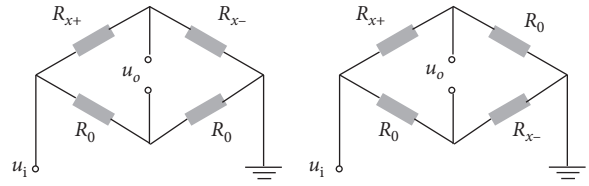

Figure 11: Structure of the Wheatstone bridges to measure the (a) bending strain and (b) axial strain.

boundary conditions. The differences between the results of different boundary conditions can also be demonstrated to be greatly dependent on the construction progress.

On the other hand, in the mentioned monitoring system, the two strain gauges in opposite directions of the same measured cross section are connected to the neighbouring arms of the Wheatstone bridges as shown in Figure 11(a) so that the bending strain (i.e., the difference between the two measured strains) can be obtained. If the two strain gauges are arranged face to face in the Wheatstone bridges as shown in Figure 10(b), the output is the summation of the measured strains. After deducting the temperature-induced drift by using a free strain gauge in the same environment, one can obtain the axial strain of the pipes, which provides a new approach to monitor the axial deformation of the structure (e.g., piles, columns, and piers). The strain gauge-based (resistance-type) deformation measurement is also economy when compared with the strategy of vibrating wire sensors and corresponding wireless readers.

4. Conclusions

To overcome the high costs of inclination measurement and other advanced strain measurements such as FBG strain sensors or vibrating wire transducers, a novel system based on economy strain gauges is proposed in this paper:

(1) All of the main components of the proposed system can be efficiently prefabricated in factory and assembled at the construction sites. Except for a main cable to provide power for measuring circuits and several short wires to connect Wheatstone bridges and the end of PCB strips, no complicated and redundant workload is needed. The accuracy and resolution of the proposed strain-based measurement are larger than those of the traditional manual method. The applicability of the mentioned system was also verified by an engineering case.

(2) It is shown that the proposed system works well to predict the vertical distribution of the lateral deflection of the supporting retaining piles (i.e., excavation wall), which is consistent with the traditional manual method. However, one should be paid special attention to that the results are sensitive to boundary conditions. The results based on measured pipes' head displacement, which is deduced from the national plane control network, are closer to "absolute" displacement but do not fit well with the traditional method that is based on the socketed condition. Moreover, special technical measures should be taken to guarantee the deformation compatibility among the strain strips, inner pipes, and outer casing pipes and then reduce the fluctuations of measured data.

(3) The method mentioned in this paper not only contributes to the thoroughly automated safety monitoring in the construction stage of underground excavations but also provides an economy and feasible approach to measure the deflection of other structures with dangerous lateral deflection or movement during their whole lifecycle, e.g., slope and high-speed railway and the axial deformation of the structure (e.g., piles, columns, and piers).

Data Availability

All data generated or analyzed during the study are included in the submitted article.

Conflicts of Interest

The authors declare that they have no conflicts of interest.

Acknowledgments

The authors acknowledge the support from the National Natural Science Foundation of China (51608139), Department of Science and Technology of Guangdong Province (2017A040405017), Guangzhou Municipal Science and Technology Bureau (201704020148), the Pearl River S&T Nova Program of Guangzhou (201806010095) and Guangzhou Municipal Construction Group Co., Ltd. ([2019]-KJ023).

References

[1] R. P. Chen, Z. C. Li, Y. M. Chen et al., "Failure investigation at a collapsed deep excavation in very sensitive organic soft clay," *Journal of Performance of Constructed Facilities*, vol. 29, no. 3, Article ID 04014078, 2015.

[2] S. Feng and S. Lu, "Failure of a retaining structure in a metro station excavation in Nanchang city, China," *Journal of Performance of Constructed Facilities*, vol. 30, no. 4, Article ID 04015097, 2016.

[3] X.-N. Gong and X.-C. Zhang, "Excavation collapse of Hangzhou subway station in soft clay and numerical investigation based on orthogonal experiment method," *Journal of*

Zhejiang University Science A, vol. 13, no. 10, pp. 760–767, 2012.

[4] K. Wardhana and F. C. Hadipriono, "Study of recent building failures in the United States," *Journal of Performance of Constructed Facilities*, vol. 17, no. 3, pp. 151–158, 2003.

[5] Y. Tan, W. Z. Jiang, W. J. Luo et al., "Longitudinal sliding event during excavation of Feng-qi station of Hangzhou metro line 1: post failure investigation," *J Journal of Performance of Constructed Facilities*, vol. 32, no. 4, Article ID 04018039, 2018.

[6] A. M. Puzrin, E. E. Alonso, and N. M. Pinyol, "Geomechanics of failures," in *Braced Excavation Collapse: Nicoll Highway, Singapore*, Springer, New York, NY, USA, 2009.

[7] MOHURD (Ministry of building and urban-rural development of the People's Republic of China), *Notification on Production Safety Accidents of Housing and Municipal Engineering in 2015*, MOHURD (Ministry of building and urban-rural development of the People's Republic of China), Beijing, China, 2016, http://www.mohurd.gov.cn/wjfb/201602/t20160218_226671.html.

[8] MOHURD (Ministry of building and urban-rural development of the People's Republic of China), *Notification on Production Safety Accidents of Housing and Municipal Engineering in 2016*, MOHURD (Ministry of building and urban-rural development of the People's Republic of China), Beijing, China, 2017, http://www.mohurd.gov.cn/wjfb/201702/t20170214_230594.html.

[9] MOHURD (Ministry of building and urban-rural development of the People's Republic of China), *Notification on Production Safety Accidents of Housing and Municipal Engineering in 2017*, MOHURD (Ministry of building and urban-rural development of the People's Republic of China), Beijing, China, 2018, http://www.mohurd.gov.cn/wjfb/201803/t20180322_235474.html.

[10] J. Hu and F. Ma, "Failure investigation at a collapsed deep open cut slope excavation in soft clay," *Geotechnical and Geological Engineering*, vol. 36, no. 1, pp. 665–683, 2018.

[11] X. S. Cheng, G. Zheng, Y. Diao et al., "Experimental study of the progressive collapse mechanism of excavations retained by cantilever piles," *Canadian Geotechnical Journal*, vol. 54, no. 4, pp. 574–587, 2017.

[12] GB50497, *Technical Code for Monitoring of Foundation Pit Engineering*, China Planning Press, Beijing, China, 2009.

[13] Y. Yu, S. Sun, and X. Y. Ni, "Advanced technologies abroad are used to improve highway construction safety," *Applied Mechanics and Materials*, vol. 737, pp. 399–403, 2015.

[14] J. W. Park, K. Kim, and Y. K. Cho, "Framework of automated construction-safety monitoring using cloud-enabled bim and ble mobile tracking sensors," *Journal of Construction Engineering and Management*, vol. 143, no. 2, Article ID 05016019, 2016.

[15] W. Zhang, A. T. C. Goh, and F. Xuan, "A simple prediction model for wall deflection caused by braced excavation in clays," *Computers and Geotechnics*, vol. 63, pp. 67–72, 2015.

[16] Anthony Teck Chee Goh, "Wengang Zhang and Anthony Teck Chee Go General behavior of braced excavation in Bukit Timah Granite residual soils: a case study," *International Journal of Geoengineering Case Histories*, vol. 3, no. 3, pp. 190–202, 2016.

[17] A. T. C. Goh, F. Zhang, W. Zhang, Y. Zhang, and H. Liu, "A simple estimation model for 3D braced excavation wall deflection," *Computers and Geotechnics*, vol. 83, pp. 106–113, 2017.

[18] W. Zhang, Y. Zhang, and A. T. C. Goh, "Multivariate adaptive regression splines for inverse analysis of soil and wall properties in braced excavation," *Tunneling and Underground Space Technology*, vol. 64, pp. 24–33, 2017.

[19] W. G. Zhang, A. T. C. Goh, K. H. Goh, O. Y. S. Chew, and R. Zhang, "Performance of braced excavation in residual soil with groundwater drawdown," *Underground Space*, vol. 3, no. 2, pp. 150–165, 2018.

[20] W. Zhang, W. Wang, D. Zhou, R. Zhang, A. T. C. Goh, and Z. Hou, "Influence of groundwater drawdown on excavation responses—a case history in Bukit Timah granitic residual soils," *Journal of Rock Mechanics and Geotechnical Engineering*, vol. 10, no. 5, pp. 856–864, 2018.

[21] W. Zhang, R. Zhang, W. Wang, F. Zhang, and A. T. C. Goh, "A Multivariate Adaptive Regression Splines model for determining horizontal wall deflection envelope for braced excavations in clays," *Tunneling and Underground Space Technology*, vol. 84, pp. 461–471, 2019.

[22] S. Li and X. Peng, "Safety monitoring of underground steel pipeline subjected to soil deformation using wireless inclinometers," *Journal of Civil Structural Health Monitoring*, vol. 6, no. 4, pp. 739–749, 2016.

[23] L. Zhao, Q. Feng, J. X. Chen, and N. Zhu, "Research on the maintenance and protection of the inclinometer and inclinometer tube in foundation ditch monitoring," *Advanced Materials Research*, vol. 645, pp. 227–231, 2013.

[24] D. W. Ha, J. M. Kim, Y. Kim, and H. S. Park, "Development and application of a wireless MEMS-based borehole inclinometer for automated measurement of ground movement," *Automation in Construction*, vol. 87, pp. 49–59, 2018.

[25] H. F. Pei, J. H. Yin, H. H. Zhu et al., "Monitoring of lateral displacements of a slope using a series of special fibre Bragg grating-based in-place inclinometers," *Measurement Science and Technology*, vol. 23, no. 2, Article ID 025007, 2012.

[26] Y.-T. Ho, A.-B. Huang, and J.-T. Lee, "Development of a fibre Bragg grating sensored ground movement monitoring system," *Measurement Science and Technology*, vol. 17, no. 7, pp. 1733–1740, 2006.

[27] C. Zhu, K. Zhang, H. Cai et al., "Combined application of optical fibers and CRLD bolts to monitor deformation of a pit-in-pit foundation," *Advances in Civil Engineering*, vol. 2019, Article ID 2572034, 16 pages, 2019.

[28] D. Liu, N. Zheng, and J. Qian, "Application research of GPS technology in vertical deformation monitoring of coal mine," *Industry and Mine Automation*, vol. 38, no. 7, pp. 14–17, 2012.

[29] G. L. Amicucci and F. Fiamingo, "Usage of RFID in safety applications," in *Proceedings of the 17th IEEE International Conference on Environment and Electrical Engineering (IEEE EEEIC) and 1st IEEE Industrial and Commercial Power Systems Europe*, Milan, Italy, June 2017.

[30] M. Pieraccini, "Extensive measurement campaign using interferometric radar," *Journal of Performance of Constructed Facilities*, vol. 31, no. 3, Article ID 04016113, 2017.